

Review

A Review on the Advancement of Ternary Alloy Counter Electrodes for Use in Dye-Sensitised Solar Cells

Edson Meyer¹, Raymond Taziwa¹, Dorcas Mutukwa^{1,2}  and Nyengerai Zingwe^{1,2,*}

¹ Fort Hare Institute of Technology, University of Fort Hare, Alice 5700, South Africa; emeyer@ufh.ac.za (E.M.); rtaziwa@ufh.ac.za (R.T.); dmutukwa@ufh.ac.za (D.M.)

² Department of Chemistry, University of Fort Hare, Alice 5700, South Africa

* Correspondence: nzingwe@ufh.ac.za; Tel.: +27-62-340-6507

Received: 23 October 2018; Accepted: 11 November 2018; Published: 19 December 2018



Abstract: A dye-sensitised solar cell (DSSC) counter electrode (CE) plays a vital role in catalysing the conversion of triiodide (I_3^-) to iodide ions (I^-), thereby ensuring the completion of the repetitive cycle of electricity generation. The platinum CE, despite being the standard counter electrode in DSSCs, has drawbacks of platinum's rarity and high cost. Platinum is an excellent redox catalyst, and consequently, it is the most sought-after metal for catalytic conversions. The huge demand for platinum in the automotive industry for vehicular catalytic converters, the pharmaceutical industry, and in oil refining, as well as other industries, has driven its price to unprecedented levels. The prohibitive price of platinum has caused newer thin film technologies, such as the DSSC which depends on the platinum CE, to be cost-ineffective, thus meaning they cannot compete with the better-established silicon-based solar cells. These problems have stagnated the development of the DSSC, which in turn has dampened larger commercialisation prospects for this thin film technology. With this in mind, this review paper focuses on recent progress in the research and development of alternative cost-effective materials to replace Pt-based CEs. Ternary alloys are amongst the possible alternatives that have been explored, yielding varied results. Alloys, especially ternary sulphides, selenides, and oxides, are attractive as alternatives as they are cheap and are easily fabricated. Ternary alloys also have a synergistic effect produced by the coexistence of two metal ions in a crystal structure, which is believed to induce greater catalytic capability, thus making them ideal cost-effective materials to replace the Pt CE in DSSCs. This review intends to highlight the performance of ternary alloy counter electrodes through the analysis of charge transfer resistance and power conversion efficiencies. Focus is also given to the restrictions and impediments to the attainment of higher power conversion efficiency in alternative CEs. The advances in fabrication of simple ternary alloys, as well as more advanced hierarchical nanostructured counter electrodes, are discussed here in detail. Results obtained to date indicate that the efficiencies of ternary alloy counter electrodes are still below that of the platinum counter electrode, and hence more research is required to enhance their efficiencies.

Keywords: dye-sensitised solar cell; counter electrode; ternary metal alloys; charge transfer resistance; power conversion efficiency

1. Introduction

With the world relying mostly on nonrenewable energy sources, such as fossil fuels, which are rapidly depleting, the rising world population and unrelenting global economic development have necessitated the need for more energy sources. The conventional energy sources are not only depleting,

but are costly, and their use has significant adverse effects on the environment [1,2]. Therefore, only renewable energy sources can fill the current global energy demand whilst limiting environmental degradation [3,4]. Amongst the renewable energy sources, solar energy is the most promising since it is abundant on earth. Despite its allure, solar cells need to be low-cost and cost-competitive in order to compete with the conventional energy sources [5]. Silicon-based solar cells with efficiencies of over 20% are the most widely used solar cells. However, the tedious fabrication processes and costly processing of materials make this solar technology expensive. Hence, it is not viable for cost-competitive generation of electricity [6]. Research efforts aimed at reducing the cost of solar cells have led to the discovery of dye-sensitised solar cells (DSSCs). DSSCs are a low-cost thin film technology which has garnered research attention for over two decades and has considerable advantages, such as simple fabrication, good performance under diffuse light conditions, higher flexibility, environmental compatibility, and low cost, compared to other thin film technologies [7–9].

The DSSC is a thin film technology that is based on mimicking the natural light harvesting process of photosynthesis in plants. It was first introduced by Gratzel and O'Regan in 1991. DSSCs consist of three adjacent thin layers, as follows: (1) a wide-bandgap photoanode semiconductor film grown or coated on a conductive substrate, e.g., TiO_2 ; (2) a sensitizer, e.g., ruthenium bipyridyl derivatives (N719 or N3); (3) an electrolyte which is sandwiched between the sensitizer and counter electrode (CE), e.g., I_3^-/I^- ; and (4) a CE which is composed of an electrocatalyst deposited on a conductive substrate, e.g., fluorine-doped tin oxide (FTO) glass substrate [10]. DSSCs have had a certified efficiency of 14.7% for a cobalt-based electrolyte and modified FTO/Au/GNP (graphene nanoplatelets) electrode since their introduction in 1991 [11].

The commercialisation potential of DSSCs is also hampered by the presence of ruthenium in the dye sensitizers and platinum in the CE, with about 50–60% of the manufacturing cost of DSSCs arising from the dye sensitizers, CE, and substrates [12]. As a result, large-scale commercialisation prospects for the DSSC have been severely affected, leading to very expensive and uneconomical prices for electricity generation. In order for solar energy to be competitive as a leading electricity generator, the functionality of the numerous solar technologies including the DSSC will have to be improved. Possible improvements to the DSSC could be achieved through: (1) replacement of the liquid electrolyte; (2) development of a dye that can absorb light from the whole visible spectrum as well as the infrared region; (3) development of an inexpensive platinum-free counter electrode that has an efficiency surpassing that of the platinum-based DSSC [13]. However, this review focuses only on the progress attained so far in the development of alternative counter electrodes to the platinum-based CE, and in particular, ternary alloys. The review also details the components that constitute a typical DSSC as well as its operating procedure. The properties of different materials and reasons why they would make excellent replacements for the platinum counter electrode are also summarised.

2. Working Principle

Under illumination from the sun, sensitizer molecules (S) in the HOMO (highest occupied molecular orbital) of the dye sensitizer become excited and absorb photons of wavelength which corresponds to the energy difference between the HOMO and LUMO (lowest occupied molecular orbital) of the dye. The excited molecules (S^*) move to the LUMO of the dye (I). These excited molecules then release photoelectrons (e^-) (II) which are transferred to the conduction band (CB) of the wide-bandgap semiconductor, leaving dye sensitizer holes (S^+) (III). The photoelectrons are transported through the semiconductor film to the conductive substrate, which in turn leads them to the CE via the external circuit (IV). At the CE, oxidised triiodide ions strip the photoelectrons, and thus they are reduced to iodide ions (V). Finally, reduced iodide ions donate electrons to the dye sensitizer holes, becoming oxidised (S^+) in the process, whilst at the same time (S^+) regenerating the dye molecules and completing the cycle of sunlight conversion into electricity (VI).

The difference between the Fermi level of the photoelectrons in the photoanode and the iodide/triiodide redox potential in the electrolyte gives the circuit voltage (V_{OC}) [13–16]. Undesirable

processes also occur, such as recombination, which occurs between the photoelectrons and the holes (S^* or I_3^- (VII and VIII, respectively), which results in the loss of efficiency in DSSCs [17]. The operational cycle can be summarised by the following Equations (1)–(6), and Figure 1 shows the operation of a DSSC.

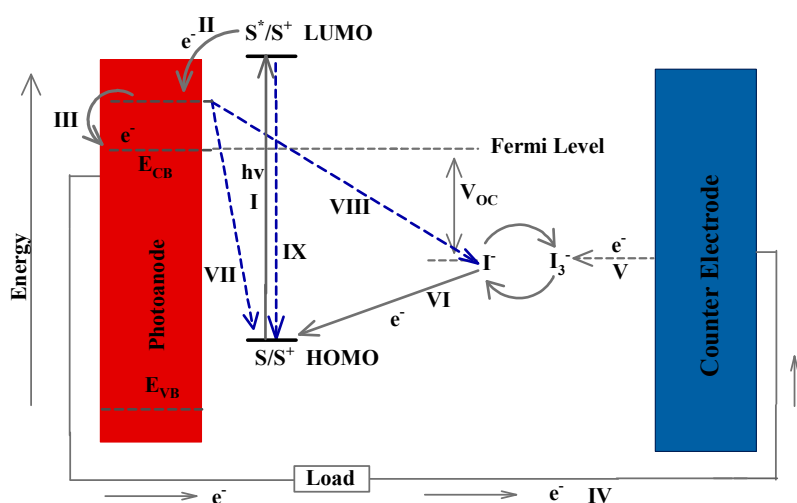
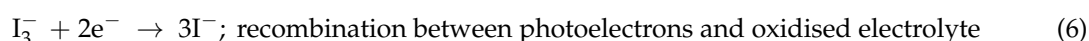
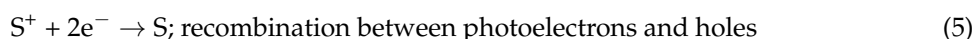
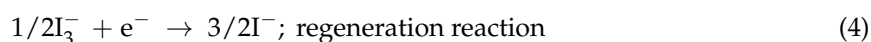
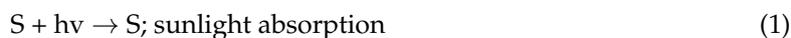


Figure 1. Illustration of the operation of a dye-sensitised solar cell (DSSC). HOMO: highest occupied molecular orbital; LUMO: lowest occupied molecular orbital. ($h\nu$ —energy, E_{CB} —conduction band level, R —resistance, V_{oc} —open circuit voltage).

All components of the cell work in sync to produce a well-functioning device. Since its invention, the DSSC has consistently underperformed, exhibiting extremely low power conversion efficiencies (PCEs); this has led to research focused on improving the individual components of the cell. The development of solid-state dye-sensitised solar cells (ssDSSCs) with solid hole conductors has sought to rid the cell of the problems associated with the liquid electrolyte [18]. Other developments which have been undertaken have sought to achieve the fabrication of a cell with an efficiency surpassing those of platinum counter electrode-based cells, whilst at the same time being a cheaper alternative. Several Pt-free CEs have been explored as possible replacements of Pt-based CEs [19–23]. Most of the materials that have been explored are good electrical conductors, although some of them do not exhibit any outstanding electrocatalytic ability [24]. Most of the materials tested were in the nanoscale range, that is the diameter of their particles were in the nanometer (nm) range, which is particularly important since nanostructured materials are believed to behave in a different manner as compared to the parent bulk material [25]. The performance of the various ternary alloy CEs explored as alternatives to platinum, and the reasons why most of them have not been able to offer satisfactory results, are outlined in the following sections.

3. Counter Electrodes

The DSSC CE enables the reduction of the triiodide ion to iodide ions, as well as being a conduit for electron transfer from the external circuit back to the oxidised dye [26]. As such, platinum was the catalyst of choice in the first invented DSSC, mainly because it exhibits greater efficiency than all the other metals with respect to its triiodide reduction capability and electron conductivity. Despite being the standard CE, platinum is very expensive and rare, such that it makes the manufacturing of DSSCs become complex. In order to rid the cell of platinum metal, resources have been diverted towards substantial research in trying to develop alternatives which are cheaper, thereby driving down costs and stimulating larger commercialisation prospects. Amongst the possible candidates have been transition metals, metal sulphides, nitrides, polymers, and alloys [27–30]. This review focuses solely on the development of ternary alloy CEs.

3.1. Ternary Metal Sulphides

Ever since Gratzel invented the DSSC, platinum has been the catalyst of choice on the counter electrode to facilitate the rapid reduction of the triiodide ion [31]. Platinum, owing to its d shell composition, is unparalleled in terms of electron conductivity and catalytic ability, especially in reduction reactions [32]. However, platinum is also very expensive. In addition, its reserves in the Earth's crust are limited, thus leading researchers to look for other cheaper alternatives whilst not sacrificing efficiency. When Gratzel fabricated a DSSC with a binary cobalt sulphide counter electrode on ITO/PEN (indium-doped tin oxide coated polyethylene naphthalene) films which produced a 6.5% power conversion efficiency (PCE), it led to widespread effort aimed at finding the right sulphide compound which could be as effective as platinum whilst withstanding corrosion from the iodine electrolyte.

Metal sulphides possess all the necessary requirements for good counter electrode activity, namely high electron conductivity and catalytic ability. Initial research undertaken to study the influence of sulphide counter electrodes on the DSSC efficiency was done on binary sulphide compounds, including CoS [33], NiS [34], MoS₂ [35], WS₂ [36], and FeS₂ [37]. Application of binary sulphide counter electrodes in DSSCs yielded varying results, as illustrated in Table 1. Amongst all the binary sulphides, CoS with a reduced graphene oxide (rGO) support yielded the best efficiency parameters, as shown in Table 1. Since cobalt and sulphur are cheap and easily accessible, CoS, if subjected to further improvement, would be deemed an ideal replacement for platinum in DSSC counter electrodes. Various methods are being used to achieve higher efficiency for binary sulphide counter electrodes; these include the use of supporting materials which enhance conductivity as well as the synthesis of hierarchical nanostructured sulphides.

Table 1. Photovoltaic parameters for various binary sulphide compounds. (R_{ct} —charge transfer resistance, R_s —sheet resistance, J_{sc} —short current density, V_{oc} —open circuit voltage, η —power conversion efficiency.)

Sample	Synthesis Method	$R_{ct}/\Omega \cdot \text{cm}^{-1}$	$R_s/\Omega \cdot \text{cm}^{-1}$	$J_{sc}/\text{mA} \cdot \text{cm}^{-2}$	V_{oc}/V	$\eta/\%$	Ref.
NiS ₂	Chemical bath deposition	5.22	7.93	12.68	0.6	5.69	[38]
NiS ₂	Solvothermal	0.81	17.66	14.11	0.77	7.39	[34]
CoS	Electrophoretic deposition	1.05	18.91	16.5	0.757	7.72	[33]
CoS	Hydrothermal	2.09	9.95	16.81	0.747	7.16	[39]
FeS ₂	Hydrothermal	5.99	2.91	12.08	0.74	5.78	[37]
Co-rGO	Hydrothermal	2.71	5.89	18.9	0.767	9.82	[40]

Although efficiencies have inched higher, other researchers have resorted to fabricating ternary sulphide catalysts in the hopes of achieving higher efficiencies, or at the very least, equalling the platinum efficiency in counter electrodes. Ternary sulphides are believed to have more superior

catalytic ability and conductivity than binary sulphides. This is attributed to the synergistic effect produced by the coexistence of two metal ions in a crystal structure, which results in greater electron conductivity and catalytic ability. Nickel-cobalt sulphides have been the most explored amongst all ternary sulphides. Most of the synthesised ternary sulphides exhibit good counter electrode properties, characterised by low charge transfer and sheet resistances, high reduction current density, and high power conversion efficiency. Initially, researchers fabricated simple ternary compounds which could be employed as counter electrode catalysts in DSSCs.

Lin et al. [41] fabricated a highly transparent NiCo_2S_4 -based counter electrode for use in a DSSC, which attained a PCE of 6.14%. Huang and associates [42] also synthesised a NiCo_2S_4 -based counter electrode which produced an 8.1% efficiency. The differences observed in PCE values for the two counter electrodes could be due to a variety of reasons, such as synthesis methods and assembly methods of the DSSCs. Therefore, to singularly determine the effect of the counter electrode on the performance of the DSSC system, analysis of its catalytic ability and conductivity are necessary. Since the counter electrode is designed to assist the reduction of the triiodide ion, thereby helping in the completion of the regeneration cycle of the dye molecules, its catalytic capability can therefore be measured by the rate at which electrons are transferred from the counter electrode surface to the electrolyte.

Determination of the rate of electron transfer or resistance to electron transfer can be achieved using several methods, which include cyclic voltammetry (CV), electrochemical impedance spectroscopy (EIS), and Tafel polarisation. Two important values from CV analysis which describe the electrocatalytic capability of the counter electrode are the reduction current density and the peak-to-peak potential difference, ΔE_{PP} . The higher the peak reduction current density, the greater the rate of reduction of the triiodide ion to iodide ions, whereas ΔE_{PP} signifies the amount of overpotential in the counter electrode. Generally, the standard electrochemical rate constant of a redox reaction is inversely proportional to ΔE_{PP} , and as such, its value should be minimum. Analysis of the ΔE_{PP} values for the two sulphide counter electrodes showed that NiCo_2S_4 -1, fabricated by Lin et al. [40], had lower over potential losses at 0.22 V, compared to 0.37 V for NiCo_2S_4 -2, fabricated by Huang et al. [41]. Consequently, the rate of reduction for NiCo_2S_4 -1 proceeded faster than for NiCo_2S_4 -2. Since the reduction current was higher for NiCo_2S_4 -1, this means that electrons encountered lower charge transfer resistance when this counter electrode was used. This is also observable in the values of the sheet resistance R_s and charge transfer resistance R_{ct} obtained from electrochemical impedance spectroscopy (EIS) analysis. PCE values for the NiCo_2S_4 -1 and NiCo_2S_4 -2 CEs show that despite having a lower ΔE_{PP} and R_{ct} as well as a higher open circuit voltage, NiCo_2S_4 -1 (NCS1) is not as efficient as NiCo_2S_4 -2 (NCS2). This signifies that the overall power conversion efficiency values of a DSSC are merely a poor indicator of the effect of the counter electrode on the DSSC. The discrepancy in PCE values could be caused by a variety of reasons, including differences in how the DSSCs were assembled, different synthesis methods, and the poor functionality of the other components of the DSSC. As clearly seen in Table 2 the PCEs of NCS1 and NCS2 are still very low compared to that of platinum; consequently, current research has sought to fabricate sulphide counter electrodes with more highly modified structures that are believed to enhance catalytic capability.

To date, many NiCo_2S_4 nanostructured compounds have been synthesised. These include microspheres [43], nanocomposites [44], nanosheets [28], nanowires [45], and nanorods. Although most of the sulphide-based catalysts have been fabricated for use in capacitors, they have also recently found widespread use in DSSCs as counter electrodes. Nanomaterials possess many outstanding qualities, such as a large electroactive surface area, larger electrolyte infiltration area, high electron transfer rate, and good structural stability. These properties improve the catalytic capability of DSSC counter electrodes. Despite all the theoretical advantages outlined, some of the results obtained experimentally are very poor, suggesting the need for further research and perhaps implementation of better synthesis methods.

Table 2. Photovoltaic parameters for various ternary sulphides. (PANI—Polyaniline).

Sample	Synthesis Method	$R_{ct}/\Omega \cdot \text{cm}^{-1}$	$R_s/\Omega \cdot \text{cm}^{-1}$	$J_{sc}/\text{mA} \cdot \text{cm}^{-2}$	V_{oc}/V	$\eta/\%$	Ref.
NiCo ₂ S ₄	Hydrothermal	4.0	10.6	17.4	0.743	8.5	[43]
NiCo ₂ S ₄ /NiS	Hydrothermal	2.2	9.6	17.7	0.744	8.8	[43]
NiCo ₂ S ₄	Solvothermal	2.4	-	14.11	0.72	6.14	[41]
rGO-NiCo ₂ S ₄	Solvothermal	0.37	9.71	16.4	0.752	8.15	[44]
NiCo ₂ S ₄	Solvothermal	0.85	10.14	15.2	0.747	7.36	[44]
NiCo ₂ S ₄	Hydrothermal	-	-	14.3	0.699	5.38	[45]
NiCo ₂ S ₄	Solvothermal	4.42	7.41	18.43	0.69	8.10	[42]
NiCo ₂ S ₄	Vulcanisation	-	-	12.17	0.763	5.81	[28]
CoNi ₂ S ₄	Hydrothermal	-	-	8.86	0.756	4.61	[46]
CuInS ₂	Bath deposition	9.65	20.49	12.48	0.78	5.79	[47]
NiCo ₂ S	Solvothermal	3.4	11.12	17.17	0.69	7.43	[48]
CuCo ₂ S ₄	Coprecipitation	13.17	-	12.04	0.495	2.97	[49]
CoS-CuS	Electrodeposition	3.04	-	16.09	0.54	5.03	[50]
CuS-NiS	Bath deposition	21.86	8.51	12.47	0.599	4.19	[51]
NiS/PANI/Ti	Electropolymerisation	1.48	5.29	14.56	0.743	7.35	[52]
ZnS-CoS	Hydrothermal	9.53	42.3	15.10	0.65	6.11	[53]
CoS-NiS	Bath deposition	2.21	7.06	11.15	0.579	3.40	[54]

Of note, Liu et al. [45] fabricated a NiCo₂S₄ nanowire array through an ion exchange reaction. Liu et al. [45] achieved PCEs of 5.35% efficiency with the DSSC technology employing NiCo₂S₄ nanowire as a CE. This counter electrode produced a short current density of 14.30 mA/cm², compared to 13.72 mA/cm² for the platinum counter electrode. The higher short current density for the NiCo₂S₄ nanowire array was attributed to the high catalytic activity for I₃⁻ reduction, which speeds up dye regeneration at the TiO₂ photoanode. Despite having a more sophisticated structure, the PCE for the NiCo₂S₄ nanowire counter electrode was actually lower than those of most binary sulphide counter electrodes. The DSSC assembled using the pure platinum counter electrode did not fare any better, with 5.92% efficiency, which is unusually low compared to other platinum counter electrodes. Therefore, since the two PCE values were very similar for the NiCo₂S₄ nanowire and the platinum counter electrode, experimental conditions as well as the means and ways of assembling the DSSCs should also be considered as efficiency determinants.

A better-functioning nanostructured NiCo₂S₄ counter electrode was developed by Huo et al. [43]. Together with associates, they synthesised flower-like nickel-cobalt sulphide microspheres modified with nickel sulphide. The NiCo₂S₄/NiS counter electrode was fabricated via a two-step hydrothermal method. In order to determine how the NiS support affected performance as well as compare its efficiency to platinum, separate NiCo₂S₄, NiS, and Pt counter electrodes were also developed. The DSSC assembled with the NiCo₂S₄/NiS counter electrode produced a modest 8.8% PCE.

CV analysis to determine its catalytic capability was characterised by a very low ΔE_{pp} , suggesting a very high rate of reduction for the triiodide ion. Figure 2 depicts curves for the cyclic voltammetry and electrochemical impedance spectroscopy analysis. As expected, a very high reduction current density was produced, further supporting the notion of its excellent catalytic activity. Since the reduction current was high, accompanied by a low ΔE_{pp} , the counter electrode was expected to exhibit very low sheet and charge transfer resistance. Charge transfer resistance values from EIS analysis illustrated the good catalytic qualities of the counter electrode, with R_{ct} and R_s values of 2.2 and 9.6 Ω , respectively. As clearly indicated in Table 2 the R_{ct} and R_s values for NiCo₂S₄/NiS were the lowest of the three platinum-free counter electrodes. The incorporation of NiS with NiCo₂S₄ to produce the NiCo₂S₄/NiS electrode improved the transfer of electrons from the counter electrode to the electrolyte. This was illustrated by the drop-in charge transfer resistance from 4 Ω for NiCo₂S₄ to 2.2 Ω for NiCo₂S₄/NiS, which is a 55% decline in resistance.

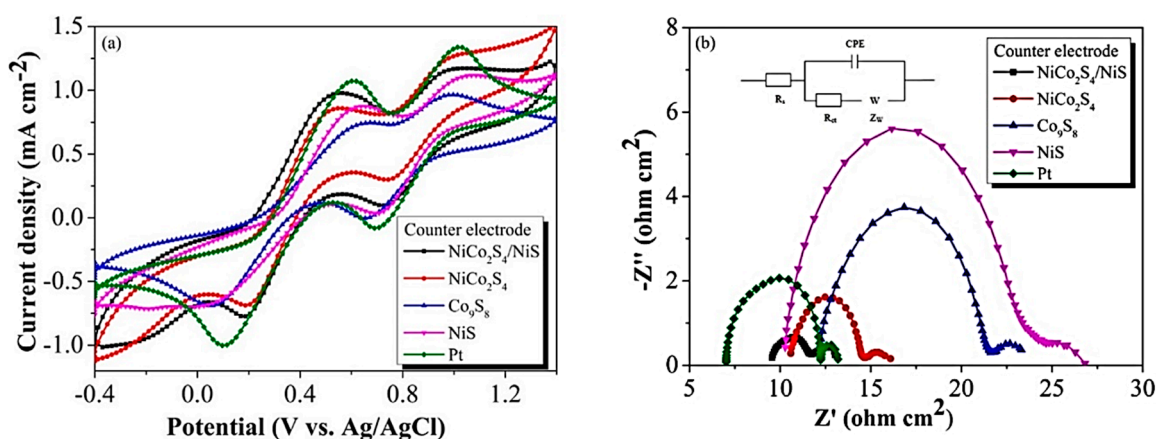


Figure 2. (a) Cyclic Voltammetry (CV) and (b) Electrochemical impedance spectroscopy (EIS) curves for NiCo₂S₄/NiS, NiCo₂S₄, Co₉S₈, NiS, and Pt electrodes. (CPE-constant phase element). Reproduced with permission from Reference [43], Elsevier 2016.

The increased transfer of charge is attributed to the fact that NiS increases the specific surface area of the microspheres, and hence more electrolyte is in contact with the counter electrode. The platinum counter electrode, despite having the highest reduction current density, possesses a high ΔE_{PP} of 504 mV, as well as a higher charge transfer resistance of 5.2 Ω . As a result, the DSSC with the NiCo₂S₄/NiS counter electrode performs better, with 8.8% PCE compared to 8.1% for platinum. As clearly shown above, the introduction of other materials could enhance the overall properties of the NiCo₂S₄ counter electrode. Most notably, carbon materials are known to be highly conductive as well as possessing a larger surface area of contact with the electrolyte. Table 3 illustrates some of the most commonly used carbon-based materials.

Table 3. Properties of various carbon-based materials. Reproduced with permission from Reference [26], Elsevier 2016.

Material	Advantages	Disadvantages
Carbon nanotubes	High electrical conductivity, large surface area	Low quantities of defective sites
Graphene	Remarkable carrier mobility, high electrical conductivity	Susceptibility to oxidative environments, low in defective sites
Carbon black	Numerous defective sites, high surface area-to-volume ratio	Low surface area, poor conductivity
Graphite	Excellent conductivity and corrosion resistance	Low surface area

The most commonly used carbon-based supporting materials include carbon nanotubes, carbon black, graphene, and graphite. Despite being touted as being highly conductive, carbon materials incorporated in DSSCs as counter electrodes have produced only moderate results, characterised by high sheet and charge transfer resistance. However, Kakiage et al. [11] reported a high efficiency of 14.7% for a graphene nanoplatelets (GNP)-based CE, which was higher than that of the Pt-based CE DSSC (13.8%). Carbon materials have, however, found more use in DSSCs as supports for other conductive materials. One such example where the introduction of a carbon-based material enhanced the properties of the counter electrode was in the work undertaken by Anuratha et al. [44]. In this work, Anuratha and associates undertook the fabrication of a NiCo₂S₄ counter electrode on a reduced graphene oxide support. The enhanced catalytic activity produced by the NiCo₂S₄-rGO counter electrode was attributed to the increased specific surface area of graphene oxide as well as its excellent electron conductivity. Anuratha et al. fabricated three counter electrodes via a one-step

solvothermal method with ratios of NiCo_2S_4 to rGO (reduced graphene oxide) equalling 1:0.3, 1:0.6, and 1:1. The reported synthesis procedure for the counter electrodes is outlined in Figure 3.

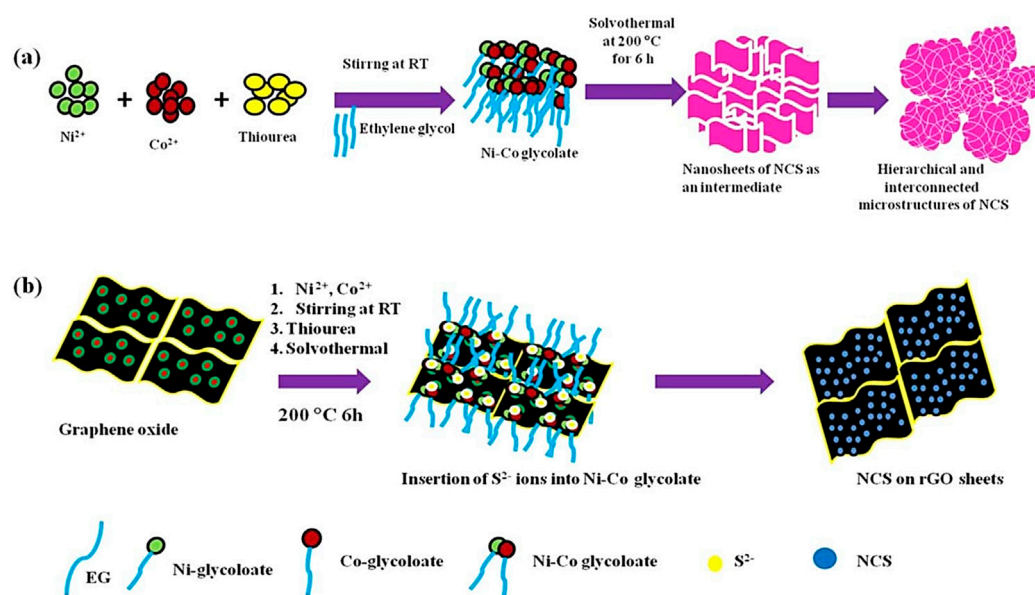


Figure 3. Schematic diagram of the NiCo_2S_4 fabrication process. (a) Nickel acetate and cobalt acetate were dissolved in ethylene glycol, to get the corresponding nickel and cobalt glycolate respectively; (b) In the case of rGO-NCS formation, GO was dispersed in EG by ultrasonication. Reproduced with permission from Reference [44], Elsevier 2017. (RT—room temperature, NCS— NiCo_2S_4 , rGO—reduced graphene oxide).

It was noted that the amount of graphene incorporated onto the counter electrode dictated the performance of the DSSC. The CV graph for rGO-NCS-2 produced the highest reduction current density, as shown in Figure 4a. Analysis of EIS data from Figure 4d shows that rGO-NCS-2 was the most catalytically active counter electrode, with the lowest charge transfer resistance of 0.37Ω . The catalytic activity of NCS, characterised by a high R_{ct} of 0.85Ω , indicates that the performance enhancement contributed by reduced graphene oxide was barely minimal. Furthermore, this work illustrates the importance of optimisation during counter electrode fabrication in order to attain the best possible performance.

At low graphene oxide levels, catalytic activity is still low, as characterised by the high R_{ct} followed by a subsequent increase to the optimum point as rGO content increases. After the optimum point has been attained, the catalytic activity dwindles as more reduced graphene oxide is deposited on the counter electrode. Higher charge transfer resistance for reduced graphene oxide at 28.22Ω implies that poor catalytic activity occurs at the counter electrode for the reduction of the triiodide ion. The stability of the synthesised counter electrodes was also measured for 20 cycles without any noticeable changes. As shown in Figure 4b–c, the shape of the cyclic voltammetry curve for NCS and rGO-NCS-2 remained virtually the same. Since photovoltaic cells normally function for a long time, it would be more ideal if the testing for stability was done for a larger number of cycles or for a lengthier period in order to ascertain their stability.

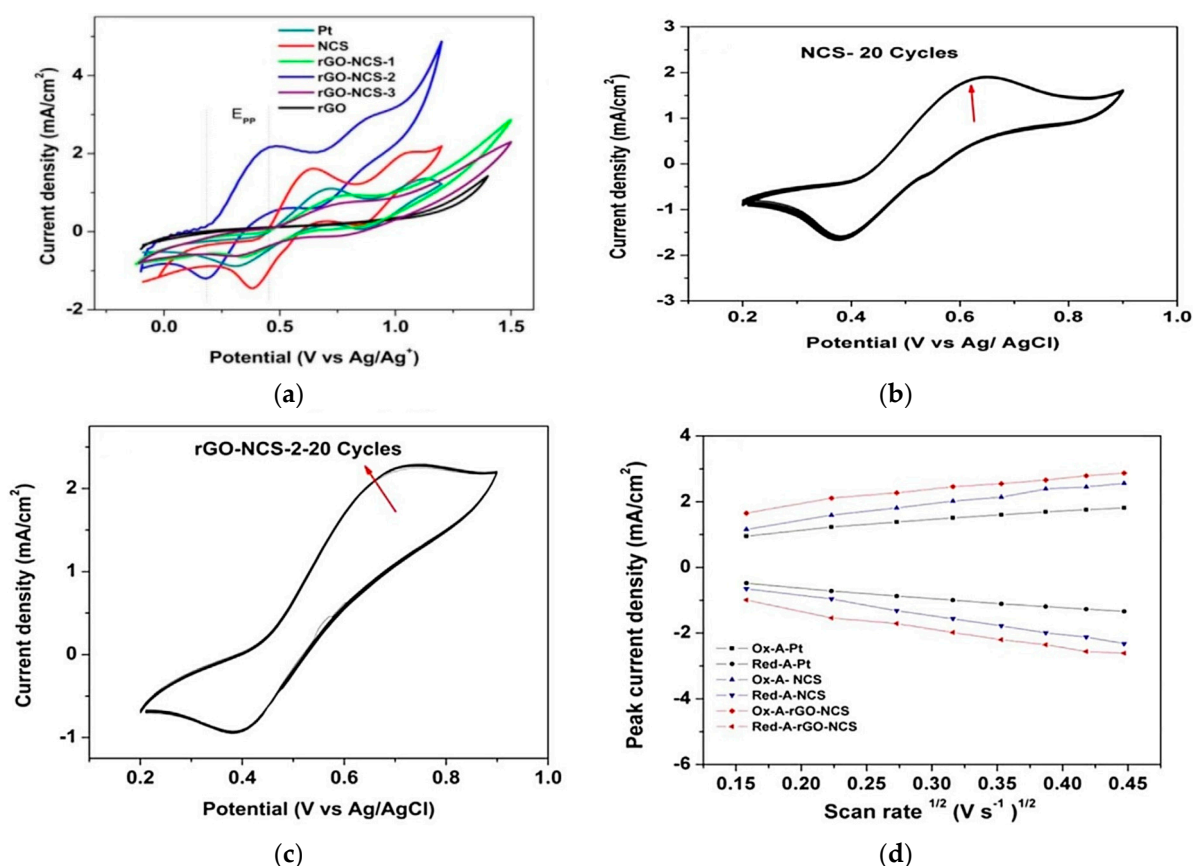


Figure 4. (a–c) CV curves for various counter electrodes and (d) their corresponding EIS curves. Reproduced with permission from Reference [44], Elsevier 2016.

Other notable suitable sulphide counter electrodes that have been developed to replace platinum include CoNi₂S₄ [46] and CuInS₂ [47]. Shi et al. [46] hydrothermally fabricated three nanostructured CoNi₂S₄ counter electrodes with different film deposition width. The most effective amongst these counter electrodes produced an efficiency of 4.61%. At lower film width, the counter electrode exhibited poor catalytic ability, and hence its cyclic voltammetry curve only had redox peaks at the positive potentials. This counter electrode consequently experienced high charge transfer resistance. The other two electrodes showed minimal charge transfer resistance characterised by low R_{ct} values. When more substrate is deposited above the optimal level of thickness, the charge transfer resistance begins to rise. Evaluation of charge transfer resistance values shows that the highest efficiency is attainable when the amount of substrate deposited on the FTO is optimal. The thicker the film of substrate deposited on the FTO, the more the resistance it encounters, whereas the lower the film thickness, the poorer the catalytic capability it exhibits.

Using liquid impregnation and carbonisation, Wang et al. [47] fabricated carbonised eggshell membranes (ESM) loaded with CuInS₂ nanocrystals. Photovoltaic parameters for the developed sample were rather low, with the power conversion efficiency for this counter electrode equalling 5.79%. Resistances to electron movement were obtained at 9.65 Ω and 20.49 Ω for R_{ct} and R_s , respectively. Since the two resistance values were high and coupled with a low PCE, CuInS₂ would not be an ideal counter electrode. Development of quantum dot-sensitised solar cells (QDSSCs) has also emancipated the fabrication of counter electrodes. Givalou et al. [50] synthesised novel cobalt-copper sulphide (CoS-CuS) counter electrodes for use in QDSSCs. The novel sulphide counter electrode produced a 5.03% efficiency.

Kim et al. [51] also fabricated a CuS-NiS composite counter electrode for use in QDSSCs. The developed counter electrode exhibited low power conversion efficiency, at 4.19%. Table 2 outlines

the performance parameters for some of the ternary sulphide counter electrodes that have been developed to date. It is evident that the most actively used methods of synthesis for ternary sulphides are hydrothermal and solvothermal synthesis. Efficiency parameters of all the sulphide counter electrodes in Table 2 are very low compared to platinum. The best-performing ternary sulphide was fabricated in a complicated three-step process, which would be very tedious for any would-be manufacturer to adopt.

Furthermore, ternary sulphides alone do not seem to possess adequate catalytic capability, and hence they require supports to enhance their catalytic ability. These supports, at times, lead to reduced catalytic activity if the thickness of the deposited film is excessive, which leads to increased sheet resistance [55]. Thus, one of the effective ways to obtain high efficiency parameters in dye-sensitised solar cells is through optimisation of the developed counter electrodes to determine the required width of film to be deposited. Considering that sulphides are abundant and easily accessible, more research is required to develop truly efficient ternary sulphide counter electrodes that can parallel platinum's capability. It is also particularly important that the most ideal method of synthesis be used to increase the probability of producing the required counter electrode that can exhibit the requisite properties to the fullest.

The continual fabrication of ternary sulphide CEs with efficiencies lower than the platinum counter electrode has led researchers to delve into the development of ternary transition metal alloys. Since platinum group metals have been proven to be catalytically superior in redox reactions, they could be incorporated with other transition metal elements that offer specific qualities which are needed by the counter electrode. These CEs could potentially function better than ternary sulphides, since each individual element has a specific contribution to the system. Development of these ternary alloys and their performance is discussed in the next subchapter.

3.2. Ternary Transition Metal Alloys

Transition metal elements have been known to partake in catalytic reactions with increased vigor than other elements in the periodic table. The use of platinum as the standard counter electrode catalyst for iodine reduction was borne from its ability to be one of the most effective reducing agents [56]. Transition metal elements, especially those with lone pairs of electrons in their d orbitals, can easily partake in redox reactions with a minimal supply of energy. As outlined earlier, researchers sought to synthesise binary metallic alloys as replacements for platinum in DSSC counter electrodes. Although most of the binary alloys have performed well, their efficiency is still far below that of a pure platinum metal CE [57,58]. However, what can be deduced so far from the work undertaken to fabricate binary metallic alloys is that the synergistic effect of the two metals creates an environment which facilitates faster charge transfer between the counter electrode and the electrolyte. Thus, in search of materials that can offer parallel performance to platinum, the fabrication of ternary metallic alloys has been extensively explored. Figure 5 shows the most commonly used transition metal elements for ternary alloy fabrication. The most commonly used elements reside in Group VIII to X. These elements have lone pairs of electrons as well as empty d orbitals, making for easy electron transfer in redox reactions.

Yang et al. [59] produced a branching NiCuPt alloy counter electrode which exhibited modest performance parameters. The NiCuPt alloy was synthesised via a three-step process, which included: (1) the electrodeposition of Ni on ZnO microrod templates, (2) the growth of Cu on the developed Ni microtubes, and (3) the galvanic displacement of Zn by Pt. Cyclic voltammetry analysis of the developed counter electrode illustrated a high reduction current density, thus good electrocatalytic activity could be expected. Furthermore, it was noted that the current density produced was dependent on the amount of galvanic displacement time the counter electrode experienced. Peak current density optimally rises to a maximum of 14.42 A within 2 h and subsequently declines for any further elongation of galvanic displacement time. The current density pattern produced in this work can be attributed to the fact that at low displacement times, not enough deposition of NiCuPt occurs. Also, after 3 h displacement time, the thickness of the deposited film becomes inhibitive to the flow of

electrons, hence high R_{ct} values should be expected as well as low PCE. Charge transfer resistance values from EIS analysis depict the same pattern, with NiCuPt after 2 h displacement (NiCuPt-2 h) having the least resistance. Subsequently, NiCuPt-2 h yields a modest 9.66% PCE, compared to 8.22% for NiCuPt-15 min. As clearly visible from this work, optimisation is essential in order to obtain the best-functioning counter electrode. Yang et al. [60] also developed a PtNiCo alloy counter electrode which displayed significant electrocatalytic capability. This counter electrode was developed via a three-step hydrothermal process similar to that illustrated in Reference [60]. Figure 6 shows SEM images of the developed PtNiCo alloy.

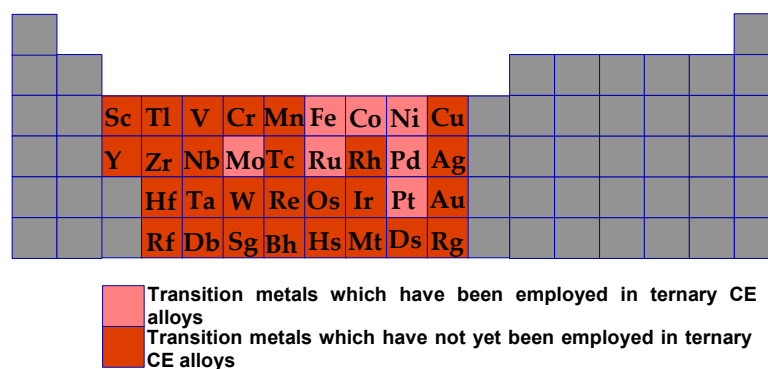


Figure 5. Periodic table illustration of the most commonly used transition metals for ternary alloy counter electrode (CE) fabrication.

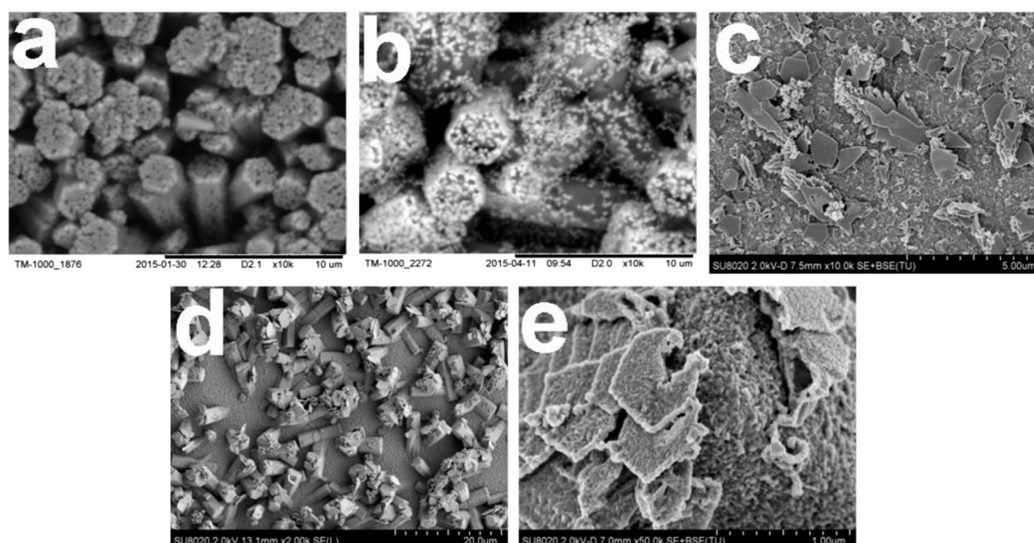


Figure 6. SEM images of (a) ZnO microrods, (b) Ni microtubes, (c) Co nanosheets, and (d,e) PtNiCo alloy. Reproduced with permission from Reference [61], Elsevier 2016.

The hexagonal ZnO microrods in Figure 6a have an average diameter of 1.5 μm . The dissolution of the ZnO microrods in sulphuric acid and subsequent addition of Ni microspheres (Figure 6b) and Co nanosheets (Figure 6c) results in the formation of the PtNiCo alloy shown in Figure 6d,e. The developed PtNiCo alloy can be described as consisting of PtCo nanosheets and PtNi nanorods. The developed counter electrode exhibited a PCE of 8.85%. CV analysis of PtNiCo produced two pairs of redox peaks with peak current density of 12.24 $\text{mA}\cdot\text{cm}^{-2}$. The ΔE_{pp} produced was also low, signifying that the rate of the reduction reaction was very high. Consequently, charge transfer between the counter electrode and the electrolyte was exceptionally fast, with resistance equalling a low 0.04 Ω , compared to 0.75 Ω for platinum.

Yang et al. [61] fabricated ternary platinum alloy counter electrodes of the composition Pt-M-Ni, where M = Co, Fe, and Pd. The three fabricated electrodes exhibited modest power conversion efficiencies, as shown here in Table 4. The three developed counter electrodes were described as having dense stacked structures. Pt-Co-Ni was homogeneously distributed on FTO, whereas the other two CEs experienced agglomeration. As a result, Pt-Co-Ni possessed lower charge transfer resistance and higher PCE since it had more active sites for electrolyte adsorption. Figure 7 depicts the morphological structure of the three counter electrodes. CV analysis of the three developed counter electrodes yielded high reduction current densities in the order Pt-Co-Ni > Pt-Pd-Ni > Pt-Fe-Ni. ΔE_{pp} values increased in the order Pt-Fe-Ni < Pt-Pd-Ni < Pt-Co-Ni. A measure of the impediment to charge transfer from the counter electrode to the electrolyte yielded a low R_{ct} for all, in the order Pt-Co-Ni < Pt-Pd-Ni < Pt-Fe-Ni < PtCo < PtPd < PtFe < Pt.

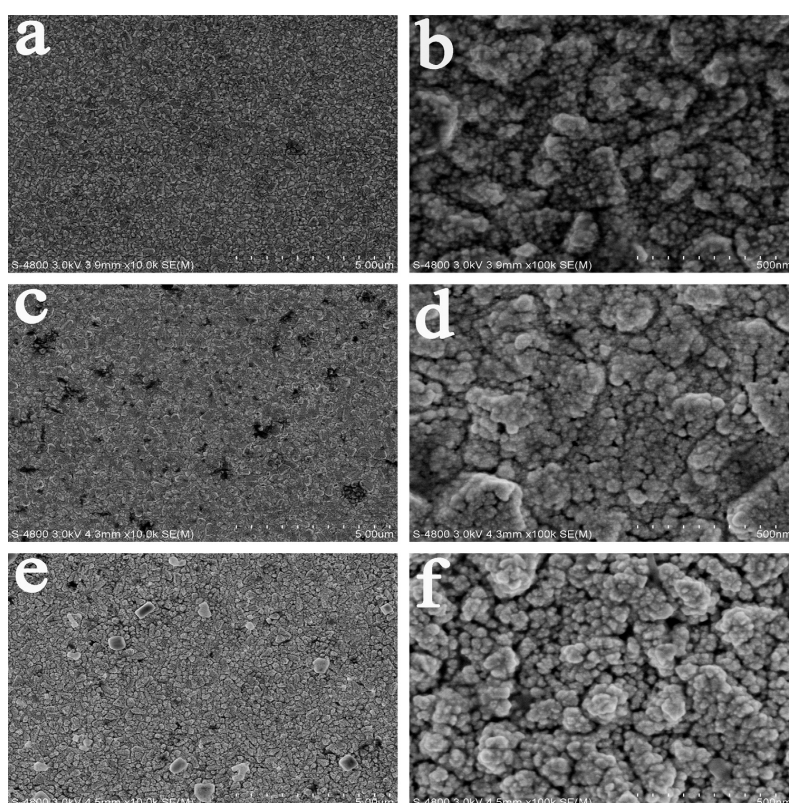


Figure 7. SEM images of ternary Pt alloy CEs. (a,b) Pt-Co-Ni, (c,d) Pt-Pd-Ni, (e,f) Pt-Fe-Ni. (Images a,c,e obtained at 5 μm while b,d,f were observed at 500 nm) Reproduced with permission from Reference [61], Elsevier 2016.

As clearly shown in Table 4, ternary alloy counter electrodes possess lower resistances to the movement of electrons in the DSSC as compared to ternary sulphide counter electrodes, as described in Table 3; consequently, their power conversion efficiencies have been reported to be higher. For example, the greater efficiency of Pt-Co-Ni compared to Pt-Pd-Ni was attributed to the matching of work functions to the redox potential of the electrolyte, leading to satisfactory catalytic activity. Matching work functions of alloy CEs are believed to induce partial electron transfer to the near surface of Pt from the transition metal atoms, leading to weakened binding energy between electrons and nucleus. These weakened electrons participate in the triiodide reduction. Impressive electrocatalytic capability and rapid electron transfer between the counter electrode and electrolyte are vital in minimising recombination reactions, thereby enhancing the overall DSSC efficiency.

Other researchers have sought to introduce nonmetallic polyaniline with binary alloy systems, since polyaniline exhibits high electrical conductivity. Polyaniline (PANI) being an electron donor,

has the potential to be an excellent counter electrode material. Although the photovoltaic parameters from DSSCs employing PANI as the counter electrode are poor, its excellent electrical properties are ideal for a support material. Since PANI also exhibits good optical transparency, it can be utilised to construct bifacial DSSCs, which have the capability of generating electricity on either side. Yu et al. [62] developed platinum alloys decorated with polyaniline. Yu et al. [62] reported three counter electrodes, namely PANI/MoPt, PANI/CoPt, and PANI/PdPt. The fabricated DSSC devices based on these three counter electrodes had efficiencies of 8.08, 7.06, and 6.83%, respectively. In order to validate whether PANI invigorates the function of the counter electrode, photovoltaic parameters for pristine PANI were also obtained. CV measurements of the four fabricated counter electrode systems yielded the highest peak current density for PANI/CoPt, with PANI possessing the lowest current density. Charge transfer resistance from the EIS analysis followed a similar trend, with PANI/CoPt possessing the lowest resistance, whilst PANI was the most inhibitive to electron flow. The excellent catalytic capability of PANI/CoPt was attributed to the similarity between its work function and that of I/I₃. The greater the difference in work function values, the greater the resistance encountered by electrons when transferring from the counter electrode to the electrolyte.

Table 4. Photovoltaic parameters for different transition metal ternary compounds. (e/c deposition—electrochemical deposition.)

Sample	Synthesis Method	$R_{ct}/\Omega \cdot \text{cm}^{-1}$	$R_s/\Omega \cdot \text{cm}^{-1}$	$J_{sc}/\text{mA} \cdot \text{cm}^{-2}$	V_{oc}/V	$\eta/\%$	Ref.
NiCuPt-2 h	Hydrothermal	0.446	-	16.0	0.758	9.66	[59]
NiCuPt-15 min	Hydrothermal	0.656	-	18.30	0.737	8.22	[59]
PtNiCo	Hydrothermal	0.640	-	17.10	0.751	8.85	[60]
PANI/CoPt	e/c deposition	1.250	2.40	16.15	0.730	8.08	[62]
PANI/PdPt	e/c deposition	8.551	2.53	15.41	0.710	7.26	[62]
PANI/MoPt	e/c deposition	9.750	2.59	15.19	0.710	6.83	[62]
PtCoNi	Cyclic voltammetry	0.660	-	17.01	0.744	8.71	[61]
PtPdNi	Cyclic voltammetry	0.810	-	16.34	0.741	8.28	[61]
PtFeNi	Cyclic voltammetry	1.010	-	16.02	0.726	7.89	[61]
CuFePt	Displacement reaction	9.540	-	15.94	0.726	8.21	[63]
CuCoPt	Displacement reaction	19.04	-	15.56	0.721	7.85	[63]
CuNiPt	Displacement reaction	26.21	-	14.84	0.720	7.30	[63]

Table 4 illustrates the wide range of synthesis methods that have been explored in ternary transition alloy fabrication. Hydrothermal synthesis of NiCuPt [59] yielded the least charge transfer resistance, and hence produced the highest power conversion efficiency. The effects of morphology on the properties of the counter electrode are shown in Figure 6, adopted from Reference [61]. Since the reduction process involves the adsorption of I₃⁻ on the counter electrode interface, its surface area and morphology must be ideal so as to offer the maximum number of catalytically active sites, thereby enhancing the reaction speed. Despite high efficiency parameters, the continued use of platinum on counter electrodes defeats the purpose of trying to reduce costs and increase mass production. Most of the ternary metallic alloys were fabricated via tedious numerous-step processes, which would be ideal for laboratory-scale operations, but highly reprehensible for large-scale production. As outlined earlier, charge transfer from the counter electrode to the electrolyte is dependent on how their work functions match. Since the work function of the CE is dependent on the alloy, it is important that the metals constituting the alloy have matching work functions whilst also complimenting each other. Ideally, the design of ternary metal alloys should be such that the three metals complement each other. For the best-performing NiCuPt CE, platinum, being the most active, would be tasked with increasing the speed of triiodide reduction. Hence, the remaining two metals, copper and nickel, should offer the other prerequisite requirements; that is, being either highly conductive, thus increasing stability in the iodine electrolyte, or increasing the surface area of contact. Further research is, however, required to determine the effects of these metals on the outlined properties. Currently, no results have been made available on this topic.

3.3. Ternary Selenides and Oxides

Metal selenides and oxides do possess high catalytic activity and good thermal properties, as well as being cheap materials [64]. Jiang et al. [65] fabricated a cobalt–nickel-based ternary selenide, $\text{Co}_x\text{Ni}_{1-x}\text{Se}$, with different cobalt and nickel ratios using the solvothermal method. The x values ranged from 0 to 1, namely 0, 0.32, 0.42, 0.52, 0.74, and 1, respectively. Figure 8a shows the CV curves of the reported synthesised counter electrodes. As can clearly be seen, $\text{Co}_{0.42}\text{Ni}_{0.58}\text{Se}$ possessed the largest reduction current density, signifying a higher triiodide reduction intensity when it is used. ΔE_{pp} was also the lowest for $\text{Co}_{0.42}\text{Ni}_{0.58}\text{Se}$, meaning that it had a faster rate of reaction amongst all the fabricated counter electrodes. The higher electrocatalytic ability of CoNiSe was attributed to the optimised synergistic effect between Co and Ni ions. To further elucidate the electrocatalytic capability of selenide counter electrodes, EIS measurements were taken, in which $\text{Co}_{0.42}\text{Ni}_{0.58}\text{Se}$ had the least charge transfer resistance at 2.95Ω . Its sheet resistance R_s was also observed to be 21.49Ω , which was far higher than 14.78Ω for platinum. This proves that platinum functions as a better electrical conductor than $\text{Co}_{0.42}\text{Ni}_{0.58}\text{Se}$. Despite its impressive electrocatalytic ability, $\text{Co}_{0.42}\text{Ni}_{0.58}\text{Se}$ had a poor 6.15% power conversion efficiency. Figure 8b illustrates the Nyquist plots for the synthesised counter electrodes.

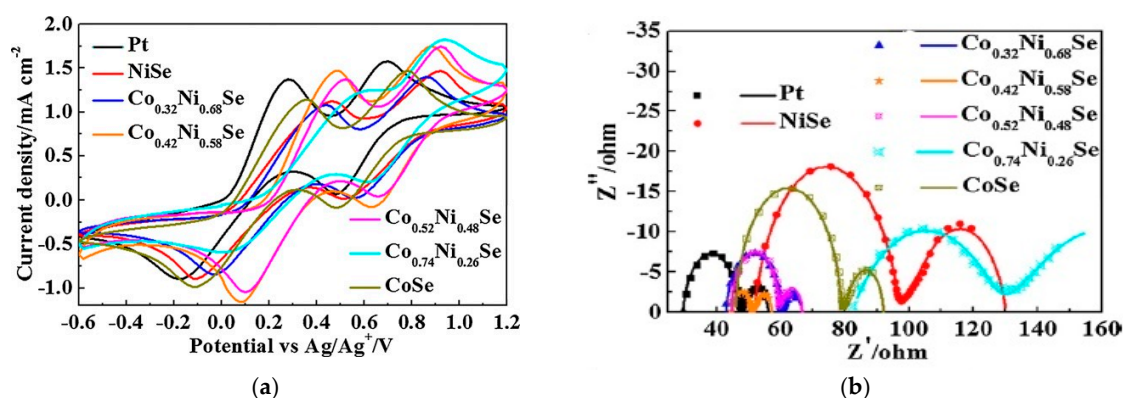


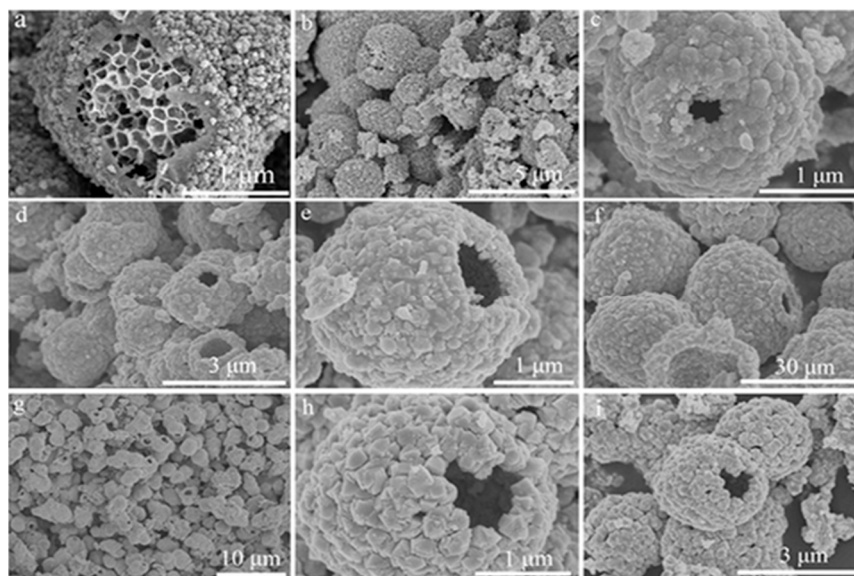
Figure 8. (a) CV and (b) EIS analysis for Pt, NiSe, $\text{Co}_{0.32}\text{Ni}_{0.68}\text{Se}$, and $\text{Co}_{0.42}\text{Ni}_{0.58}\text{Se}$ electrodes. Reproduced with permission from Reference [65], Elsevier 2017.

Other researchers have been successful in synthesising selenide counter electrodes with higher power conversion efficiencies. Shao et al. [66] developed ternary NiCoSe hollow microspheres which could be excellent counter electrodes in DSSC. Shao et al. [66] fabricated four NiCoSe counter electrodes at varying temperatures via the hydrothermal method. The compositions of the four developed counter electrodes are outlined in Table 5. From the CV curves obtained, NiCoSe-180 °C had the highest reduction current density as well as the lowest peak-to-peak difference. Charge transfer resistance from EIS analysis proved NiCoSe-180 °C was catalytically superior compared to other counter electrodes, with 1.27Ω resistance. Consequently, NiCoSe-180 °C possessed the highest power conversion efficiency at 9.04%. From Table 5, it can clearly be seen that catalytic performance increases as temperature increases up to 180 °C and subsequently decreases for any further increase in temperature. At temperatures below 180 °C, the formation of irregular hollow spheres occurs, whereas at temperatures above 200 °C, the hollow structures collapse and deform due to the sustained high temperatures.

At temperatures $\approx 180 \text{ }^\circ\text{C}$, the formation of regular hollow structures composed of homogeneous rough nanoparticles occurs, which provide effective transport pathways for the rapid transportation of electrons and ions, leading to enhanced electrochemical kinetics. Figure 9 illustrates how the shape of microspheres vary with temperature. Table 5 illustrates how the amount of cobalt present in each counter electrode determines its catalytic prowess.

Table 5. Variation of the atomic percentages of Ni, Co, and Se with charge transfer resistance and power conversion efficiency.

CE	Ni	Co	Se	$R_{ct}/\Omega \cdot \text{cm}^{-1}$	$\eta/\%$	Ref.
NiCoSe-140 °C	0	4.58	30.41	11.3	7.41	[66]
NiCoSe-160 °C	3.79	4.88	33.22	2.05	8.39	[66]
NiCoSe-180 °C	7.25	10.39	51.93	1.27	9.04	[66]
NiCoSe-200 °C	8.28	9.36	31.76	1.68	8.72	[66]

**Figure 9.** SEM images of NiCoSe-140 °C (a,b), NiCoSe-160 °C (c,d), NiCoSe-180 °C (e,f), and NiCoSe-200 °C (h,i). Reproduced with permission from Reference [66], Elsevier 2017.

The power conversion efficiency trend for the four electrodes mirrors the trend in cobalt composition. Efforts to replace platinum with ternary oxides have also been explored. Du et al. [67] hydrothermally fabricated NiCo_2O_4 for application in dye-sensitised solar cell counter electrodes. In this work, through morphology manipulation, Du and associates developed and optimised new structures with more open channels, thereby facilitating easier electron and ion movement. The newly developed structures were nanoflowers, nanosheets, and nanorods. Power conversion efficiencies for the three developed structures equalled 8.48, 3.57, and 6.48%, respectively. Charge transfer and sheet resistance were, as expected, the lowest for NiCo_2O_4 nanoflowers, at 0.35 and 4.94 Ω , respectively. These values signify that NiCo_2O_4 nanoflowers have excellent reduction capability for triiodide ions as well as good conductivity. Analysis of the effect of hydrothermal reaction time on cell efficiency shows that for shorter reaction periods, the power conversion efficiency was relatively weak, whereas after 12 h reaction time, the PCE was 8.48%. Thus, efficiency increases with an increase in reaction time. In order to improve the function of the NiCo_2O_4 counter electrodes, Wang et al. [68] explored the combination of the ternary oxide with carbon black. This counter electrode achieved an efficiency of 6.27% to 7.38% for the platinum counter electrode. EIS analysis of the counter electrode yielded a 2.2 Ω charge transfer resistance, compared to 1.8 Ω for platinum. The NiCo_2O_4 /carbon black composite counter electrode is still below the standard required to replace the platinum counter electrode. Further research is required to improve its efficiency. Perhaps the inclusion of carbon nanotubes in this composite rather than carbon black would produce satisfactory results.

Table 6 illustrates the dominance of the hydrothermal method in ternary alloy fabrication. Efficiencies obtained using this method are still very low, thus making the process less attractive

since it is very expensive. Further research is required to elevate the efficiencies of ternary selenides and oxides.

Table 6. Photovoltaic parameters for different ternary selenides and oxides.

Sample	Synthesis Method	$R_{ct}/\Omega \cdot \text{cm}^{-1}$	$R_s/\Omega \cdot \text{cm}^{-1}$	$J_{sc}/\text{mA} \cdot \text{cm}^{-2}$	V_{oc}/V	$\eta/\%$	Ref.
$\text{Co}_{0.42}\text{Ni}_{0.58}\text{Se}$	Solvothermal	2.95	22.46	14.79	0.66	6.15	[64]
NiCo_2O_4 nanoflowers	Hydrothermal	0.35	4.94	17.01	0.77	8.48	[66]
NiCo_2O_4 nanosheets	Hydrothermal	20.94	3.72	12.2	0.79	3.57	[66]
NiCo_2O_4 nanorods	Hydrothermal	0.8	3.38	15.08	0.77	6.84	[66]
NiCo_2O_4	Hydrothermal	2.2	-	-	-	6.27	[67]
$\text{NiCoSe-180}^\circ\text{C}$	Hydrothermal	1.27	10.3	17.78	0.77	9.04	[65]
$\text{NiCoSe-140}^\circ\text{C}$	Hydrothermal	11.3	10.3	14.74	0.79	7.41	[65]
$\text{NiCoSe-160}^\circ\text{C}$	Hydrothermal	2.05	10.1	16.55	0.757	8.39	[65]
$\text{NiCoSe-200}^\circ\text{C}$	Hydrothermal	1.68	10.7	17.74	0.76	8.72	[65]

The effect of the price of platinum on the large-scale use of the DSSC technology is clearly illustrated in Table 7. The price of platinum per gram is substantially higher than for any other substance, except carbon nanotubes. Platinum's high price, which is always fluctuating because of widespread demand, would not be sustainable for CE manufacture, and consequently, the DSSC technology could not compete with silicon-based solar cells as the best solar energy generation technology. Table 7 also illustrates the quandary associated with carbon nanotubes, where the advanced nature and infancy of their development makes them equally expensive for use in DSSCs. Therefore, compatible solutions to eliminate the high-cost factor of platinum would be to employ cheaper sulphides or metal alloys such as NiCo or PtRu, which consist of limited amounts of platinum. To date, most of the platinum-free counter electrodes that have been developed have performed at lower efficiencies compared to the platinum counter electrode. The most vital factors determining catalytic activity are the morphology and specific area of the catalyst. As such, the development of catalysts on carbon supports, such as carbon black or graphene, which offer higher specific area will improve catalytic performance. Anuratha et al. [44] developed a rGO-NiCo₂S₄ which had a higher PCE at 8.15%, compared to 7.37% for NiCo₂S₄. Furthermore, the atomic distribution in higher metallic alloys has a great influence on its catalytic activity. Taking PdNiCo as an example, the more catalytically active palladium should be distributed in such a manner as to have greater contact with the electrolyte, thereby influencing its catalytic ability. One possible way of achieving this is through synthesis of alloys with a core-shell structure, where the more active metal comprises the shell, or in hollow structures, which guarantee a high specific surface area-to-volume ratio.

Table 7. Variation of cost and efficiency for different counter electrode materials.

Compound	Efficiency	Price \$US/g (Sigma Aldrich)	Ref.
Platinum	13.8	480	[11]
NiS	7.39	5.84	[34]
Carbon nanotubes	6.41	1000	[69]
NiCo	4.47	0.03	[70]
CoS	7.72	10.8	[33]
FeS	5.78	0.252	[37]
Carbon black	8.35	40	[71]
PtRu	6.80	162	[57]

4. Stability

One of the most critical prerequisites for the practical applicability of dye-sensitised solar cells is their long-term stability. Since DSSCs are required to operate in often harsh weather conditions, it is vital that they are able to withstand all these conditions. The most significant stability concerns

associated with DSSCs include dissociation of the thin catalyst film on the CE and corrosion of the iodine electrolyte, as well as leakage of the electrolyte. Stability of the CE is determined by cyclic voltammetry through evaluation of changes in reduction current density and peak potential difference. Since the peak potential difference between the oxidation and reduction peaks in CV analysis gives an indication of electrocatalytic ability, any changes in that peak potential difference can be evaluated to give insight as to its effect on electrocatalytic ability.

In order to ascertain CE stability, Yang et al. [59] carried out 100 stacked CVs for two alloys, namely NiCuPt-2 h and NiCuPt-15 min. Deteriorating catalytic activity in NiCuPt-15 min resulted in a 49.5% decline in reduction current density from 12.79 to 6.92 $\text{mA}\cdot\text{cm}^{-2}$, whilst NiCuPt-2 h did not undergo any reduction current decline. Figure 10a,c illustrates the results of the cyclic voltammetry evaluation for the two counter electrodes. Evaluation of the long-term stability of the assembled DSSC was achieved through alternatively irradiating ($100\text{ mW}\cdot\text{cm}^{-2}$) and darkening ($0\text{ mW}\cdot\text{cm}^{-2}$) the cell at 25 s intervals. In this work, Yang et al. [59] observed that photocurrent density increased during irradiation, signifying higher conductivity and catalytic activity at the CE. Under persistent irradiation for 2000 s, current density for NiCuPt-2 h decreased from 14.87 to 13.45 $\text{mA}\cdot\text{cm}^{-2}$. Figure 11 shows the results of the stability analysis for the assembled DSSC.

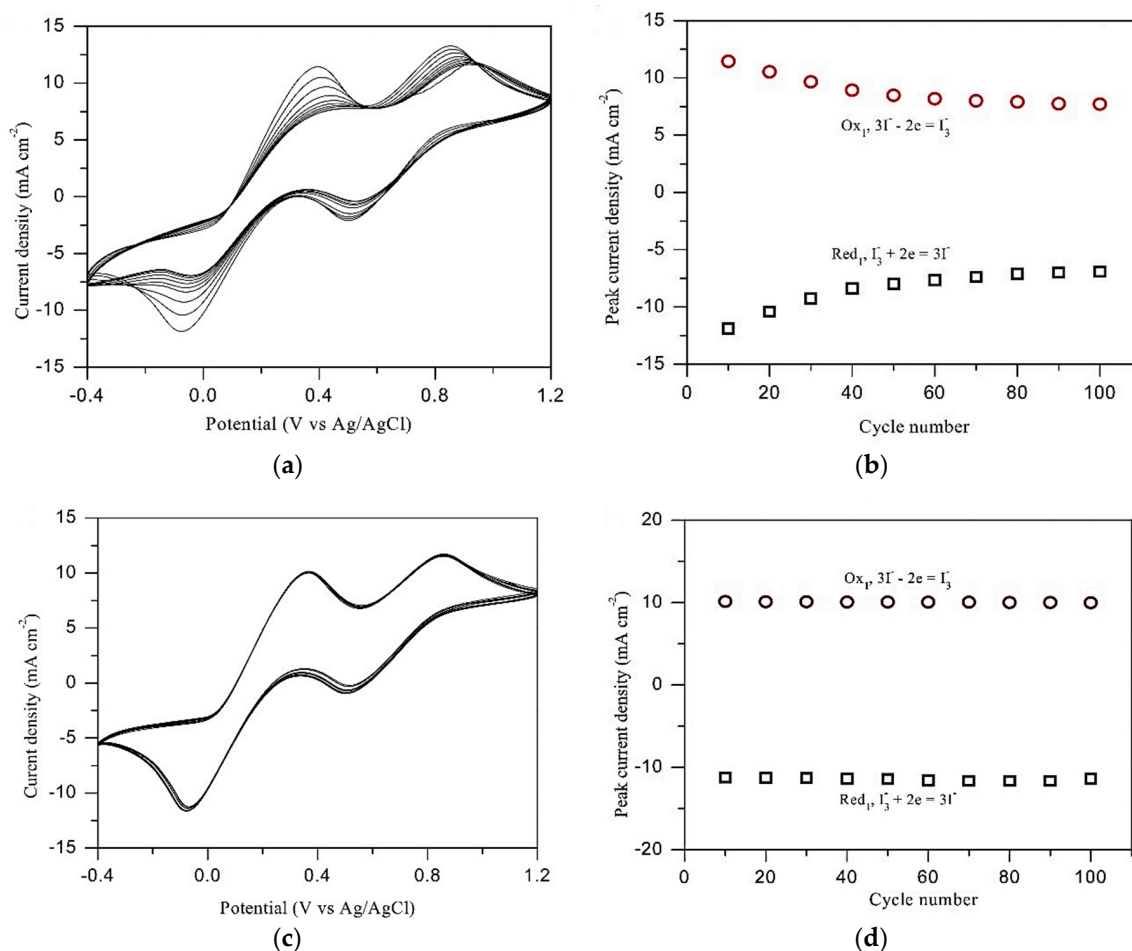


Figure 10. The 100 stacked CV curves and evolution of reduction current density J_{red} as a function of cycle number for the (a,b) NiCuPt-15 min CE and the (c,d) NiCuPt-2 h CE. Reproduced with permission from Reference [60], Elsevier 2016.

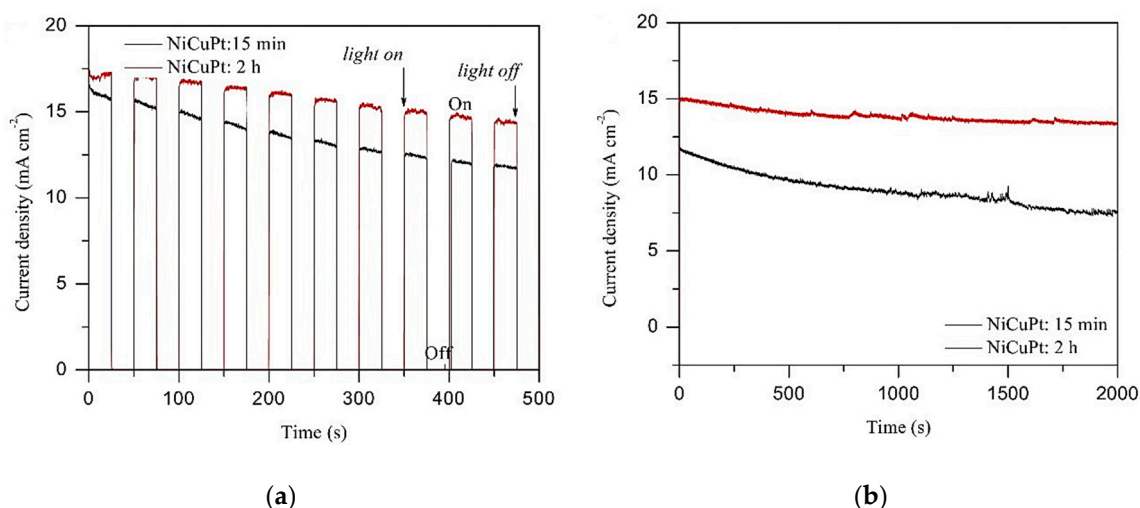


Figure 11. (a) On-off switches of DSSCs made by alternatively illuminating ($100 \text{ mW}\cdot\text{cm}^{-2}$) and darkening ($0 \text{ mW}\cdot\text{cm}^{-2}$) the devices; (b) Photocurrent stabilities of the DSSC devices with different CEs under durable irradiations at $100 \text{ mW}\cdot\text{cm}^{-2}$. Reproduced with permission from Reference [60], Elsevier 2016.

Yang et al. [60] also probed the stability of the PtNiCo alloy. After 10 CV cycles, the PtNiCo displayed only a 2.6% decrease in current density, compared to 9.4% for the pure platinum CE. Figure 12 shows the current density stability of the two CEs at $100 \text{ mW}\cdot\text{cm}^{-2}$ irradiation. The platinum counter electrode subsequently underwent a 0.89% current density reduction. As clearly illustrated, most of the CEs developed for use in DSSCs displayed excellent stability in shorter stability testing periods, whereas when exposed to prolonged periods of testing, electrocatalytic capability subsequently declined. Thus, in order to ascertain how stable CEs are, it is vital that stability tests be undertaken for longer time periods.

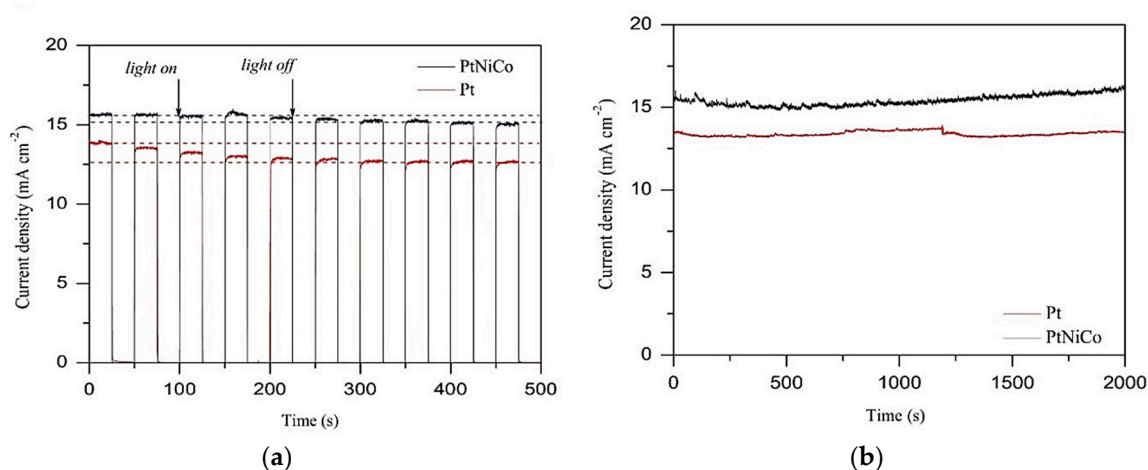


Figure 12. (a) The on-off switches of the DSSCs under alternative irradiation at 100 and $0 \text{ mW}\cdot\text{cm}^{-2}$; (b) Photocurrent stability of the DSSC at $100 \text{ mW}\cdot\text{cm}^{-2}$. Reproduced with permission from Reference [61], Elsevier 2016.

5. Conclusions

The dye-sensitised solar cell remains one of the most promising photovoltaic technologies to be invented. However, inadequacies associated with the cost of manufacture as well as limited photo to current conversion efficiency have stifled the widespread use of the dye-sensitised solar cell. Existence of the ruthenium-based dye and the platinum counter electrode influences the cost

of the dye-sensitised solar cell. Numerous alternatives to the platinum counter electrode have been explored, producing varied power conversion efficiencies. This review paper has shown that ternary transition alloys produced the best catalytic performances, with efficiencies of 9.66%, 8.85%, and 8.71% for NiCuPt, PtNiCo, and PtCoNi, respectively, compared to ternary metal sulphides, selenides, and oxides, with moderate efficiencies of 8.8%, 8.72%, and 8.48% for NiCoS₄/NiS, NiCoSe-200 °C, and NiCo₂O₄ nanoflowers, respectively. Ternary sulphides, selenides, and oxides have also shown great promise. Moreover, the easy access and affordability of ternary sulphides makes them ideal candidates for counter electrode electrocatalysts. Lower efficiencies in sulphides were shown to be greatly improved in the presence of ideal supports. Overall, more research is required to produce truly effective platinum-free counter electrodes, and understanding of the effect of particle size, composition, and shape on performance should be gained. Furthermore, enhancement of fabrication techniques and optimisation of the developed electrocatalysts are vital for the development of efficient and cost-effective dye-sensitised solar cells.

Author Contributions: Conceptualisation, N.Z. and D.M.; Writing—review and editing, N.Z. and D.M.; Visualisation, R.T.; Supervision, R.T.; Funding acquisition, E.M.

Funding: This research was funded by the South African National Research Foundation (NRF) and the South African Department of Science and Technology (DST). We also extend our sincere gratitude to the Govan Mbeki Research and Development Centre (GMRDC) at the University of Fort Hare for their support.

Acknowledgments: We are grateful for financial support from our sponsors: The South African National Research Foundation (NRF), Department of Science & Technology (DST), Eskom tertiary education support (TESP), and Govan Mbeki Research & Development Centre (GMRDC) of the University of Fort Hare.

Conflicts of Interest: The authors declare no conflict of interest.

References

1. Panwar, N.L.; Kaushik, S.C.; Kothari, S. Role of renewable energy sources in environmental protection: A review. *Renew. Sustain. Energy Rev.* **2011**, *15*, 1513–1524. [[CrossRef](#)]
2. Ali, N.; Ali, N.; Hussain, A.; Ahmed, R.; Wang, M.K.; Zhao, C.; Haq, B.U.; Fu, Y.Q. Advances in nanostructured thin film materials for solar cell applications. *Renew. Sustain. Energy Rev.* **2016**, *59*, 726–737. [[CrossRef](#)]
3. Ellabban, O.; Abu-Rub, H.; Blaabjerg, F. Renewable energy resources: Current status, future prospects and their enabling technology. *Renew. Sustain. Energy Rev.* **2014**, *39*, 748–764. [[CrossRef](#)]
4. Azad, A.K.; Rasul, M.G.; K Khan, M.M.; Ahasan, T.; Ahmed, S.F. Energy Scenario: Production, consumption and prospect of renewable energy in Australia. *J. Power Energy Eng.* **2014**, *22*, 19–2519. [[CrossRef](#)]
5. Ye, M.; Wen, X.; Wang, M.; Iocozzia, J.; Zhang, N.; Lin, C.; Lin, Z. Recent advances in dye-sensitized solar cells: From photoanodes, sensitizers and electrolytes to counter electrodes. *Mater. Today* **2015**, *18*, 155–162. [[CrossRef](#)]
6. Razykov, T.M.; Ferekides, C.S.; Morel, D.; Stefanakos, E.; Ullal, H.S.; Upadhyaya, H.M. Solar photovoltaic electricity: Current status and future prospects. *Sol. Energy* **2011**, *85*, 1580–1608. [[CrossRef](#)]
7. Wei, D. Dye sensitized solar cells. *Int. J. Mol. Sci.* **2010**, *11*, 1103–1113. [[CrossRef](#)]
8. Jena, A.; Kumar, P.; Naduvath, J.; Gondane, V.; Lekha, P.; Das, J.; Narula, H.K.; Mallick, S.; Bhargava, P. Dye sensitized solar cells: A review. *Trans. Indian Ceram. Soc.* **2012**, *71*, 1–16. [[CrossRef](#)]
9. Kutraleeswaran, M.; Venkatachalam, M.; Saroja, M.; Gowthaman, P.; Shankar, S. Dye sensitized solar cells—A Review. *J. Adv. Res. Appl. Sci.* **2017**, *4*, 26–38.
10. Lee, C.-P.; Lin, R.Y.-Y.; Lin, L.-Y.; Li, C.-T.; Chu, T.-C.; Sun, S.-S.; Lin, J.T.; Ho, K.-C. Recent progress in organic sensitizers for dye-sensitized solar cells. *RSC Adv.* **2015**, *5*, 23810–23825. [[CrossRef](#)]
11. Kakiage, K.; Aoyama, Y.; Yano, T.; Oya, K.; Fujisawa, J.I.; Hanaya, M. Highly-efficient dye-sensitized solar cells with collaborative sensitization by silyl-anchor and carboxy-anchor dyes. *Chem. Commun.* **2015**, *51*, 15894–15897. [[CrossRef](#)]
12. Mozaffari, S.; Nateghi, M.R.; Zarandi, M.B. An overview of the challenges in the commercialization of dye sensitized solar cells. *Renew. Sustain. Energy Rev.* **2017**, *71*, 675–686. [[CrossRef](#)]

13. Jiao, Y.; Zhang, F.; Meng, S. Dye sensitized solar cells principles and new design. *Sol. Cells-Dye Devices* **2011**, 131–148. [[CrossRef](#)]
14. Grätzel, M. Dye-sensitized solar cells. *J. Photochem. Photobiol. C Photochem. Rev.* **2003**, *4*, 145–153. [[CrossRef](#)]
15. Kong, F.-T.; Dai, S.-Y.; Wang, K.-J. Review of recent progress in dye-sensitized solar cells. *Adv. Optoelectron.* **2007**, *2007*, 1–13. [[CrossRef](#)]
16. Ludin, N.A.; Mahmoud, A.M.A.-A.; Mohamad, A.B.; Kadhum, A.A.H.; Sopian, K.; Karim, N.S.A. Review on the development of natural dye photosensitizer for dye-sensitized solar cells. *Renew. Sustain. Energy Rev.* **2014**, *31*, 386–396. [[CrossRef](#)]
17. Gao, C.; Han, Q.; Wu, M. Review on transition metal compounds based counter electrode for dye-sensitized solar cells. *J. Energy Chem.* **2018**, *27*, 703–712. [[CrossRef](#)]
18. Park, N.G. Perovskite solar cells: An emerging photovoltaic technology. *Mater. Today* **2015**, *18*, 65–72. [[CrossRef](#)]
19. Li, L.; Sui, H.; Zhao, K.; Zhang, W.; Li, X.; Liu, S. Preparation of carbon nano fibers supported MoO₂ composites electrode materials for application in dye-sensitized solar cells. *Electrochim. Acta* **2018**, *259*, 188–195. [[CrossRef](#)]
20. Li, P.; Zhang, Y.; Yang, X.; Gao, Y.; Ge, S. Alloyed PtNi counter electrodes for high-performance dye-sensitized solar cell applications. *J. Alloys Compd.* **2017**, *725*, 1272–1281. [[CrossRef](#)]
21. Hamed, W.A.; Rahman, M.S.; Mahmud, H.N.M.E.; Yahya, R.; Sulaiman, K.; Mahmud, H.N.M.E.; Yahya, R.; Sulaiman, K. Processable dodecylbenzene sulfonic acid (DBSA) doped poly (N-vinyl carbazole)-poly(pyrrole) for optoelectronic applications. *Des. Monomers Polym.* **2017**, *20*, 1–10. [[CrossRef](#)]
22. Cha, S.M.; Nagaraju, G.; Sekhar, S.C.; Bharat, L.K.; Yu, J.S. Fallen leaves derived honeycomb-like porous carbon as a metal-free and low-cost counter electrode for dye-sensitized solar cells with excellent tri-iodide reduction. *J. Colloid Interface Sci.* **2018**, *513*, 843–851. [[CrossRef](#)]
23. Gao, C.; Wang, H.; Han, Q.; Hu, Z.; Wu, M. High efficiency magnetic carbon spheres counter electrode for dye-sensitized solar cell. *Electrochim. Acta* **2018**, *264*, 312–318. [[CrossRef](#)]
24. Liu, T.; Zhao, Y.; Duan, J.; He, B.; Zheng, J.; Tang, Q. Transparent ternary alloy counter electrodes for high-efficiency bifacial dye-sensitized solar cells. *Sol. Energy* **2018**, *170*, 762–768. [[CrossRef](#)]
25. Zheng, W.; Qi, T.; Zhang, Y.; Shi, H.; Tian, J. Fabrication and characterization of a multi-walled carbon nanotube-based counter electrode for dye-sensitized solar cells. *New Carbon Mater.* **2015**, *30*, 391–396. [[CrossRef](#)]
26. Chen, M.; Shao, L. Review on the recent progress of carbon counter electrodes for dye-sensitized solar cells. *Chem. Eng. J.* **2016**, *304*, 629–645. [[CrossRef](#)]
27. Li, Q.; Wu, J.; Tang, Q.; Lan, Z.; Li, P.; Lin, J.; Fan, L. Application of microporous polyaniline counter electrode for dye-sensitized solar cells. *Electrochem. Commun.* **2008**, *10*, 1299–1302. [[CrossRef](#)]
28. Liu, K.; Wei, A.; Liu, J.; Liu, Z.; Xiao, Z.; Zhao, Y. NiCo₂S₄ nanosheet thin film counter electrodes prepared by a two-step approach for dye-sensitized solar cells. *Mater. Lett.* **2018**, *217*, 185–188. [[CrossRef](#)]
29. Qiu, J.; He, D.; Zhao, R.; Sun, B.; Ji, H.; Zhang, N.; Li, Y.; Lu, X.; Wang, C. Fabrication of highly dispersed ultrafine Co₉S₈ nanoparticles on carbon nanofibers as low-cost counter electrode for dye-sensitized solar cells. *J. Colloid Interface Sci.* **2018**, *522*, 95–103. [[CrossRef](#)]
30. Zhang, X.; Hao, Y.; Shang, C.; Chen, X.; Li, W.; Hu, S.; Cui, G. Coaxial titanium vanadium nitride core e sheath nano fibers with enhanced electrocatalytic activity for triiodide reduction in dye-sensitized solar cells. *Electrochim. Acta* **2018**, *271*, 388–396. [[CrossRef](#)]
31. O'Regan, B.; Gratzel, M. A low-cost, high-efficiency solar-cell based on dye-sensitized colloidal TiO₂ films. *Nature* **1991**, *353*, 737–740. [[CrossRef](#)]
32. Bond, G.C. Platinum metals as hydrogenation catalysts. *Platin. Met. Rev.* **1957**, *1*, 87–93.
33. Huo, J.; Zheng, M.; Tu, Y.; Wu, J.; Hu, L.; Dai, S. A high performance cobalt sulphide counter electrode for dye-sensitized solar cells. *Electrochim. Acta* **2015**, *159*, 166–173. [[CrossRef](#)]
34. Zhou, W.; Jia, X.; Chen, L.; Yin, Z.; Zhang, Z.; Gao, G. Low cost NiS as an efficient counter electrode for dye-sensitized solar cells. *Mater. Lett.* **2016**, *163*, 1–3. [[CrossRef](#)]
35. He, B.; Zhang, X.; Zhang, H.; Li, J.; Meng, Q.; Tang, Q. Transparent molybdenum sulphide decorated polyaniline complex counter electrodes for efficient bifacial dye-sensitized solar cells. *Sol. Energy* **2017**, *147*, 470–478. [[CrossRef](#)]

36. Li, S.; Chen, Z.; Zhang, W. Dye-sensitized solar cells based on WS₂ counter electrodes. *Mater. Lett.* **2012**, *72*, 22–24. [[CrossRef](#)]
37. Song, C.; Wang, S.; Dong, W.; Fang, X.; Shao, J.; Zhu, J.; Pan, X. Hydrothermal synthesis of iron pyrite (FeS₂) as efficient counter electrodes for dye-sensitized solar cells. *Sol. Energy* **2016**, *133*, 429–436. [[CrossRef](#)]
38. Punnoose, D.; Kim, H.J.; Kumar, C.S.S.P.; Rao, S.S.; Gopi, C.V.V.M.; Chung, S.H. Highly catalytic nickel sulphide counter electrode for dye-sensitized solar cells. *J. Photochem. Photobiol. A Chem.* **2015**, *306*, 41–46. [[CrossRef](#)]
39. Xiao, Y.; Han, G.; Chang, Y.; Zhang, Y.; Lin, J.Y. Cobalt sulphide counter electrodes enhanced by a hydro-thermal treatment for use in platinum-free dye-sensitized solar cells. *Mater. Res. Bull.* **2015**, *68*, 9–15. [[CrossRef](#)]
40. Huo, J.; Wu, J.; Zheng, M.; Tu, Y.; Lan, Z. A transparent cobalt sulphide/reduced graphene oxide nanostructure counter electrode for high efficient dye-sensitized solar cells. *Electrochim. Acta* **2016**, *187*, 210–217. [[CrossRef](#)]
41. Lin, J.Y.; Chou, S.W. Highly transparent NiCo₂S₄ thin film as an effective catalyst toward triiodide reduction in dye-sensitized solar cells. *Electrochem. Commun.* **2013**, *37*, 11–14. [[CrossRef](#)]
42. Huang, N.; Zhang, S.; Huang, H.; Liu, J.; Sun, Y.; Sun, P.; Bao, C.; Zheng, L.; Sun, X.; Zhao, X. Pt-sputtering-like NiCo₂S₄ counter electrode for efficient dye-sensitized solar cells. *Electrochim. Acta* **2016**, *192*, 521–528. [[CrossRef](#)]
43. Huo, J.; Wu, J.; Zheng, M.; Tu, Y.; Lan, Z. Flower-like nickel cobalt sulphide microspheres modified with nickel sulphide as Pt-free counter electrode for dye-sensitized solar cells. *J. Power Sources* **2016**, *304*, 266–272. [[CrossRef](#)]
44. Anuratha, K.S.; Ramaprakash, M.; Panda, S.K.; Mohan, S. Studies on synergetic effect of rGO-NiCo₂S₄ nanocomposite as an effective counter electrode material for DSSC. *Ceram. Int.* **2017**, *43*, 10174–10182. [[CrossRef](#)]
45. Liu, J.; Li, C.; Zhao, Y.; Wei, A.; Liu, Z. Synthesis of NiCo₂S₄ nanowire arrays through ion exchange reaction and their application in Pt-free counter-electrode. *Mater. Lett.* **2016**, *166*, 154–157. [[CrossRef](#)]
46. Shi, Z.; Deng, K.; Li, L. Pt-free and efficient counter electrode with nanostructured CoNi₂S₄ for dye-sensitized solar cells. *Sci. Rep.* **2015**, *2–7*. [[CrossRef](#)] [[PubMed](#)]
47. Wang, L.; He, J.; Zhou, M.; Zhao, S.; Wang, Q.; Ding, B. Copper indium disulphide nanocrystals supported on carbonized chicken eggshell membranes as efficient counter electrodes for dye-sensitized solar cells. *J. Power Sources* **2016**, *315*, 79–85. [[CrossRef](#)]
48. Huang, N.; Li, G.; Huang, H.; Sun, P.; Xiong, T.; Xia, Z.; Zheng, F.; Xu, J.; Sun, X. One-step solvothermal tailoring the compositions and phases of nickel cobalt sulphides on conducting oxide substrates as counter electrodes for efficient dye-sensitized solar cells. *Appl. Surf. Sci.* **2016**, *390*, 847–855. [[CrossRef](#)]
49. Buckley, A.N.; Skinner, W.M.; Harmer, S.L.; Pring, A.; Fan, L.J. Electronic environments in carrollite, CuCo₂S₄, determined by soft X-ray photoelectron and absorption spectroscopy. *Geochim. Cosmochim. Acta* **2009**, *73*, 4452–4467. [[CrossRef](#)]
50. Givalou, L.; Antoniadou, M.; Perganti, D.; Giannouri, M.; Karagianni, C.S.; Kontos, A.G.; Falaras, P. Electrodeposited cobalt-copper sulphide counter electrodes for highly efficient quantum dot sensitized solar cells. *Electrochim. Acta* **2016**, *210*, 630–638. [[CrossRef](#)]
51. Kim, H.J.; Suh, S.M.; Rao, S.S.; Punnoose, D.; Tulasivarma, C.V.; Gopi, C.V.V.M.; Kundakarla, N.; Ravi, S.; Durga, I.K. Investigation on novel CuS/NiS composite counter electrode for hindering charge recombination in quantum dot sensitized solar cells. *J. Electroanal. Chem.* **2016**, *777*, 123–132. [[CrossRef](#)]
52. Yue, G.; Tan, F.; Li, F.; Chen, C.; Zhang, W.; Wu, J.; Li, Q. Enhanced performance of flexible dye-sensitized solar cell based on nickel sulphide/polyaniline/titanium counter electrode. *Electrochim. Acta* **2014**, *149*, 117–125. [[CrossRef](#)]
53. Yao, F.; Sun, P.; Sun, X.; Huang, N.; Ban, X.; Huang, H.; Wen, D.; Liu, S.; Sun, Y. One-step hydrothermal synthesis of ZnS-CoS microcomposite as low cost counter electrode for dye-sensitized solar cells. *Appl. Surf. Sci.* **2016**, *363*, 459–465. [[CrossRef](#)]
54. Kim, H.J.; Kim, S.W.; Gopi, C.V.V.M.; Kim, S.K.; Rao, S.S.; Jeong, M.S. Improved performance of quantum dot-sensitized solar cells adopting a highly efficient cobalt sulphide/nickel sulphide composite thin film counter electrode. *J. Power Sources* **2014**, *268*, 163–170. [[CrossRef](#)]

55. Guarracino, F.; Cabrini, L.; Baldassarri, R.; Petronio, S.; De Carlo, M.; Covello, R.D.; Landoni, G.; Gabbriellini, L.; Ambrosino, N. Noninvasive ventilation for awake percutaneous aortic valve implantation in high-risk respiratory patients: A case series. *J. Cardiothorac. Vasc. Anesth.* **2010**, *294*, 3124–3130. [[CrossRef](#)] [[PubMed](#)]
56. Bond, B.G.C. Periodic Variations in the catalytic properties of metals. *Platin. Met. Rev.* **2005**, *12*, 100–105.
57. Cai, H.; Tang, Q.; He, B.; Li, P. PtRu nanofiber alloy counter electrodes for dye-sensitized solar cells. *J. Power Sources* **2014**, *258*, 117–121. [[CrossRef](#)]
58. Li, Y.; Tang, Q.; Yu, L.; Yan, X.; Dong, L. Cost-effective platinum alloy counter electrodes for liquid-junction dye-sensitized solar cells. *J. Power Sources* **2016**, *305*, 217–224. [[CrossRef](#)]
59. Yang, P.; Tang, Q. A branching NiCuPt alloy counter electrode for high-efficiency dye-sensitized solar cell. *Appl. Surf. Sci.* **2016**, *362*, 28–34. [[CrossRef](#)]
60. Yang, P.; Tang, Q. Alloying of Pt with Ni microtubes and Co nanosheets for counter electrode of dye-sensitized solar cell. *Mater. Lett.* **2016**, *164*, 206–209. [[CrossRef](#)]
61. Yang, Q.; Yang, P.; Duan, J.; Wang, X.; Wang, L.; Wang, Z.; Tang, Q. Ternary platinum alloy counter electrodes for high-efficiency dye-sensitized solar cells. *Electrochim. Acta* **2016**, *190*, 85–91. [[CrossRef](#)]
62. Yu, Y.; Tang, Q.; He, B.; Chen, H.; Zhang, Z.; Yu, L. Platinum alloy decorated polyaniline counter electrodes for dye-sensitized solar cells. *Electrochim. Acta* **2016**, *190*, 76–84. [[CrossRef](#)]
63. Duan, J.; Tang, Q.; Zhang, H.; Meng, Y.; Yu, L.; Yang, P. Counter electrode electrocatalysts from one-dimensional coaxial alloy nanowires for efficient dye-sensitized solar cells. *J. Power Sources* **2016**, *302*, 361–368. [[CrossRef](#)]
64. Jia, J.; Wu, J.; Tu, Y.; Huo, J.; Zheng, M.; Lin, J. Transparent nickel selenide used as counter electrode in high efficient dye-sensitized solar cells. *J. Alloys Compd.* **2015**, *640*, 29–33. [[CrossRef](#)]
65. Jiang, Q.; Pan, K.; Lee, C.S.; Hu, G.; Zhou, Y. Cobalt-nickel based ternary selenides as high-efficiency counter electrode materials for dye-sensitized solar cells. *Electrochim. Acta* **2017**, *235*, 672–679. [[CrossRef](#)]
66. Shao, L.; Qian, X.; Li, H.; Xu, C.; Hou, L. Shape-controllable syntheses of ternary Ni-Co-Se alloy hollow microspheres as highly efficient catalytic materials for dye-sensitized solar cells. *Chem. Eng. J.* **2017**, *315*, 562–572. [[CrossRef](#)]
67. Du, F.; Yang, Q.; Qin, T.; Li, G. Morphology-controlled growth of NiCo₂O₄ ternary oxides and their application in dye-sensitized solar cells as counter electrodes. *Sol. Energy* **2017**, *146*, 125–130. [[CrossRef](#)]
68. Wang, Y.; Fu, N.; Ma, P.; Fang, Y.; Peng, L.; Zhou, X.; Lin, Y. Facile synthesis of NiCo₂O₄/carbon black composite as counter electrode for dye-sensitized solar cells. *Appl. Surf. Sci.* **2017**, *419*, 670–677. [[CrossRef](#)]
69. Yue, G.; Wu, J.; Lin, J.Y.; Xiao, Y.; Tai, S.Y.; Lin, J.; Huang, M.; Lan, Z. A counter electrode of multi-wall carbon nanotubes decorated with tungsten sulphide used in dye-sensitized solar cells. *Carbon N. Y.* **2013**, *55*, 1–9. [[CrossRef](#)]
70. Motlak, M.; Barakat, N.A.M.; Akhtar, M.S.; Hamza, A.M.; Kim, B.S.; Kim, C.S.; Khalil, K.A.; Almajid, A.A. High performance of NiCo nanoparticles-doped carbon nanofibers as counter electrode for dye-sensitized solar cells. *Electrochim. Acta* **2015**, *160*, 1–6. [[CrossRef](#)]
71. Wu, C.S.; Chang, T.W.; Teng, H.; Lee, Y.L. High performance carbon black counter electrodes for dye-sensitized solar cells. *Energy* **2016**, *115*, 513–518. [[CrossRef](#)]

